Analytic Study of the Modulation Response of Reflective Semiconductor Optical Amplifiers

Cristian Antonelli, Antonio Mecozzi, *Fellow, IEEE, Fellow, OSA*, Zhefeng Hu, and Marco Santagiustina, *Member, IEEE*

***Abstract*—We study the modulation response of a reflective semiconductor optical amplifier (RSOA) operated by directly modulating its injection current. We derive an analytic expression for the 3 dB modulation bandwidth, and characterize its dependence on the main RSOA parameters. Our study is based on a reduced model for the nonlinear RSOA response.**

***Index Terms*—Nonlinear optics, optical communications, pulse propagation models, reflective semiconductor optical amplifiers.**

I. Introduction

An important requirement for the implementation of WDM-based next-generation optical access networks is the availability of efficient, colorless optical network units [1]. Reflective semiconductor optical amplifiers (RSOAs) are considered excellent candidates to fulfil this requirement, as they can be seeded from remote nodes, providing significant amplification over the entire C-band. As well known, the performance of RSOAs that are operated by directly modulating the injection current depends primarily on their modulation bandwidth, a limiting factor which is typically imputed to the long carrier lifetime [2], [3]. The experimental characterization of this critical parameter was performed in several works [3]–[7], showing that the bandwidth has a non trivial dependence on the RSOA structural parameters. On the other hand, the dependence on the operational parameters is much better understood, being essentially dominated by an increase of the bandwidth with the injection current and the optical power. In order to give explanations to the experimental results, a number of models have been proposed [3], [6], [8], [9]. In those models several phenomena occurring in the semiconductor can be taken into account in great detail: various carrier-hole recombination effects, nonlinear gain saturation, the spatial dependence of the parameters etc. However, the equations governing such detailed models can only be solved through time consuming numerical integrations, an approach that does not enable to rapidly grasp an insight into the dependence of the RSOA response on its parameters. Theoretical studies of RSOAs' modulation bandwidth—equivalent to the work of Mork *et al.* in the context of single-pass SOAs [10]—seem to be absent in the literature.

In this paper we study the modulation response of a RSOA. By targeting applications related to optical access networks, we consider a scheme where the RSOA is seeded by an optical CW field, and the data are encoded in the RSOA optical output power by modulating the injection current. We present an analytic characterization of the RSOA output, and derive an expression for the 3 dB modulation bandwidth. Our analysis allows to effectively characterize the dependence of the modulation bandwidth on the main RSOA parameters and to gain insight on this dependence. Eventually, we compare the dynamics of SOAs in single-pass and reflective configurations and show that a RSOA is equivalent to a longer SOA featuring a reduced saturation energy. The present study is based on a simplified model for the nonlinear dynamics of RSOAs, recently introduced by Antonelli and Mecozzi [11], here extended so as to account for the RSOA internal loss and partial mirror reflectivity.

II. Reduced Model for the RSOA Nonlinear Dynamics

Lightwave propagation in a RSOA is described by a set of two coupled equations for the electric field dynamics and one equation for the gain dynamics,

$$\frac{\partial \tilde{E}_+}{\partial z} = -\frac{1}{v_g}\frac{\partial \tilde{E}_+}{\partial t} - \frac{\alpha_i}{2}\tilde{E}_+ + \frac{(1-i\alpha)g\tilde{E}_+}{2} \tag{1}$$

$$\frac{\partial \tilde{E}_-}{\partial z} = \frac{1}{v_g}\frac{\partial \tilde{E}_-}{\partial t} + \frac{\alpha_i}{2}\tilde{E}_- - \frac{(1-i\alpha)g\tilde{E}_-}{2} \tag{2}$$

$$\frac{\partial g}{\partial t} = -\frac{g-g_0}{\tau} - \frac{1}{E_{\rm sat}}\frac{|\tilde{E}_+|^2+|\tilde{E}_-|^2}{1+\epsilon\left(|\tilde{E}_+|^2+|\tilde{E}_-|^2\right)}g. \tag{3}$$

Here we denote by $\tilde{E}_+(z,t)$ and $\tilde{E}_-(z,t)$ the complex envelopes of the forward and backward propagating fields, respectively. The parameter v_g is the group velocity in the semiconductor material, α is the linewidth enhancement factor and α_i is the RSOA internal loss coefficient. By $g(z,t)$ we denote the gain coefficient, related to the carrier density N by

$$g = \Gamma a(N-N_0), \tag{4}$$

where a is the differential gain, Γ is the confinement factor and N_0 the carrier density required for transparency. The linear

Manuscript received December 2, 2014; revised May 11, 2015 and June 11, 2015; accepted June 22, 2015. Date of publication July 19, 2015; date of current version September 12, 2015. This work was supported by the Italian Ministry of University and Research through ROAD-NGN project (PRIN 2010/2011). The work of C. Antonelli and A. Mecozzi was supported by the Italian Government under Cipe resolution no. 135 (December 21, 2012), project INnovating City Planning through Information and Communication Technologies. The work of Z. Hu and M. Santagiustina was held in the framework of the agreement with ISCOM, Rome. The work of Z. Hu was supported by the Fundamental Research Funds for the Central Universities (ZYGX2012J008).

C. Antonelli and A. Mecozzi are with the Department of Physical and Chemical Sciences, University of L'Aquila, L'Aquila 67100, Italy (e-mail: cristian.antonelli@univaq.it; antonio.mecozzi@univaq.it).

Z. Hu and M. Santagiustina are with the Department of Information Engineering, University of Padova, Padova 35131, Italy (e-mail: zfhu@uestc.edu.cn; marco.santagiustina@unipd.it).

Color versions of one or more of the figures in this paper are available online at http://ieeexplore.ieee.org.

Digital Object Identifier 10.1109/JLT.2015.2453232

dependence of the gain coefficient on carrier density is rather accurate for bulk materials, which we assume in this work [12]. Quantum well-based RSOAs are better characterized by a logarithmic gain function, which however is incompatible with the formulation of a reduced model, and hence requires a fully numerical approach [9]. The parameter g_0 is the small-signal gain coefficient, related to the other RSOA parameters through

$$g_0 = \Gamma a \tau \mathcal{R}(N_0) \left(\frac{I}{I_0} - 1 \right), \tag{5}$$

where $\mathcal{R}(N)$ is the carrier decay rate, and $\tau = (\mathrm{d}\mathcal{R}/\mathrm{d}N|_{N=N_0})^{-1}$ is the carrier lifetime. By $I_0 = q_e V \mathcal{R}(N_0)$ we denote the transparency injection current, where q_e is the electron charge, V is the active volume and I is the actual injection current. We note that the definitions of g_0, τ, and I_0 introduced above are based on the linearization of the carrier decay rate function $\mathcal{R}(N)$ around the transparency carrier density N_0, according to $\mathcal{R}(N) \simeq \mathcal{R}(N_0) + (\mathrm{d}\mathcal{R}/\mathrm{d}N|_{N=N_0})(N - N_0)$. The quantity ϵ is the nonlinear gain suppression parameter, and finally E_{sat} is the RSOA saturation energy that is related to the other RSOA parameters through $E_{\mathrm{sat}} = \hbar\omega_0 A/(\Gamma a)$, where A is the area of the semiconductor active region and ω_0 is the lightwave angular frequency [13].

Note that Eqs. (1)–(3) do not account explicitly for the interference between the counterpropagating fields $\tilde{E}_+$ and $\tilde{E}_-$. In fact, due to the fast carrier diffusion, the effective contribution of the cavity standing wave to the gain saturation can be assumed to be included in the nonlinear gain suppression parameter [14].

The integration of Eqs. (1)–(3) is customarily pursued through a numerical approach, owing to the absence of known analytic solutions. However, in the case of a SOA, the space-time model reduces rigourously to a one-dimensional model when the nonlinear gain saturation and the SOA internal loss can be neglected ($\epsilon = 0, \alpha_i = 0$) [13].

Recently, this simplification has been extended to the study of the perfect reflective configuration, where the reduced model describing the nonlinear dynamics in a lossless RSOA consists of a delayed differential equation (DDE), which simplifies to an ordinary differential equation (ODE) when the effect of the propagation delay in the RSOA can be ignored [11]. In a recent publication [15], the ODE reduced model has been further improved to account for the RSOA internal loss. In the appendix of this paper we show how the DDE model can also be extended to include internal losses and partial mirror reflectivity.

Note that throughout this work we will still neglect nonlinear gain suppression and set $\epsilon = 0$. In fact, in the regime of low-to-moderate saturation that we consider in the present study, this simplifying assumption is valid if the signal bandwidth is below a critical value of the order of $f_{\mathrm{cr}} = v_g a/\epsilon$ [16]. For typical SOA parameters [9] f_{cr} exceeds 100 GHz, that is a value significantly larger than the typical RSOA modulation bandwidth (a few Gigahertz). We verified that, for a range of parameter values significantly broader than that considered in this work, the numerical solutions of the space-time model do not change significantly when the nonlinear gain suppression is included. Let us remark that, though the reduced model could be extended so as to include nonlinear gain suppression in the regime of low-to-moderate RSOA saturation by following the procedure presented in [16], the only approach to study the regime of strong saturation is the numerical one [9].

The derivation of the simplified DDE and ODE models for $\alpha_i \neq 0$ and for partial mirror reflectivity is somewhat involved and is presented in the appendix. The result is that the complex envelope of the electric field at the RSOA output, $E_{\mathrm{out}}(t)$, can be expressed in terms of the input electric field $E_{\mathrm{in}}(t)$ as follows:

$$\begin{aligned} E_{\mathrm{out}}(t) = \ & \sqrt{R} \exp\left\{ \frac{1 - i\alpha}{2} \left[h(t - t_g) + h(t - 2t_g) \right] \right. \\ & \left. - \alpha_i L \right\} E_{\mathrm{in}}(t - 2t_g), \end{aligned} \tag{6}$$

where R is the power reflection coefficient of the RSOA rear facet and $h(t)$ is the integrated gain function (see Eqs. 39 and 40) which is obtained by solving the following DDE:

$$\begin{aligned} \frac{\mathrm{d}h(t)}{\mathrm{d}t} = \ & -\frac{h(t) - g_0 L}{\tau} + \\ & - \frac{1}{E_{\mathrm{sat}}} \frac{h(t)}{h(t) - \alpha_i L} \left\{ \exp\left[h(t) - \alpha_i L \right] - 1 \right\} \\ & \left\{ |E_{\mathrm{in}}(t)|^2 + R \exp\left[h(t - t_g) \right. \right. \\ & \left. \left. - \alpha_i L \right] |E_{\mathrm{in}}(t - t_g)|^2 \right\}, \end{aligned} \tag{7}$$

with initial condition $h(t) = g_0 L$ for $t \leq 0$, and where $t_g = L/v_g$ is the one-way group delay, with L denoting the semiconductor length. In order to simplify the equations, in what follows the functional dependence on time of the integrated gain is indicated explicitly only if the integrated gain is evaluated at a delayed time. The result of [15] is recovered by setting $t_g = 0$ in Eq. (7), which gives the simpler ODE model,

$$\begin{aligned} \frac{\mathrm{d}h}{\mathrm{d}t} = \ & -\frac{h - g_0 L}{\tau} - \frac{1}{E_{\mathrm{sat}}} \frac{h}{h - \alpha_i L} \left[\exp\left(h - \alpha_i L \right) - 1 \right] \\ & \left[1 + R \exp\left(h - \alpha_i L \right) \right] |E_{\mathrm{in}}(t)|^2. \end{aligned} \tag{8}$$

Note that the lossless case, with total reflection at rear facet, which is described by Eqs. (15) and (16) of [11], is recovered by setting $\alpha_i = 0$ and $R = 1$ in Eq. (8).

III. Small-Signal Analysis

We study the output power of a directly modulated RSOA when a CW optical field is injected from the front facet. The modulation of the injection current I produces a modulation of the small-signal gain coefficient g_0 owing to Eq. (5). We express the modulated current as

$$I(t) = \overline{I} + \Delta I \exp\left(-i\Omega t \right) + \Delta I^* \exp\left(i\Omega t \right), \tag{9}$$

where $\overline{I}$ is the average injection current and ΔI is the complex envelope of the small modulation. The corresponding gain modulation can be expressed similarly,

$$g_0(t) = \overline{g}_0 + \Delta g \exp\left(-i\Omega t \right) + \Delta g^* \exp\left(i\Omega t \right), \tag{10}$$

with $\overline{g}_0 = \Gamma a N_0 (\overline{I}/I_0 - 1)$ and $\Delta g = \Gamma a N_0 \Delta I / I_0$. The resulting modulation of the electric field can be described in terms

of a small modulation of the integrated gain $h(t)$, which we express as

$$h(t) = h_0 + \Delta h \exp(-i\Omega t) + \Delta h^* \exp(i\Omega t). \quad (11)$$

Denoting by $P_{\rm in}$ the optical power of the CW field injected in the RSOA, Eqs. (6) and (11) yield the output power in the following form:

$$P_{\rm out}(t) = P_{\rm in} R \exp\left[2h_0 - 2\alpha_i L + K\cos(\Omega t - \Phi)\right], \quad (12)$$

where

$$K = 2\left|\Delta h\left[1 + \exp(i\Omega t_g)\right]\right| \quad (13)$$

$$\Phi = \text{Phase}\left\{\Delta h \exp(i\Omega t_g)\left[1 + \exp(i\Omega t_g)\right]\right\}. \quad (14)$$

By using the Jacobi–Anger expansion [17] in the form $\exp[K\cos(\phi)] = \sum_{n=-\infty}^{+\infty} I_n(K)\exp(in\phi)$, where by I_n we denote the modified Bessel function of the first kind of order n [17], Eq. (12) can be readily expressed as the Fourier series

$$P_{\rm out}(t) = \sum_{n=-\infty}^{+\infty} P_n \exp(-in\Omega t), \quad (15)$$

with coefficients

$$P_n = P_{\rm in} R \exp(2h_0 - 2\alpha_i L)\, I_n(K) \exp(in\Phi). \quad (16)$$

A. Determination of h_0 and Δh

We now proceed to the calculation of h_0 and Δh. To this aim we substitute Eqs. (10) and (11) into Eq. (7) for the DDE model, and into Eq. (8) for the ODE model, also setting $|E_{\rm in}(t)|^2 = P_{\rm in}$. After expanding the right-hand sides of the two equations to first order with respect to Δh, as appropriate in the context of a perturbative analysis, we then equate separately the constant terms and the terms that are proportional to $\exp\{\pm i\Omega t\}$. As a result of this procedure the average integrated gain h_0 is found to be the solution of the same transcendental equation for both reduced models,

$$\frac{h_0 - \overline{g}_0 L}{\tau} = -\frac{P_{\rm in}}{E_{\rm sat}} \frac{h_0}{h_0 - \alpha_i L}\left[\exp(h_0 - \alpha_i L) - 1\right] \left[1 + R\exp(h_0 - \alpha_i L)\right]. \quad (17)$$

Note that actually h_0 solution of Eq. (17) describes the static gain for a DC RSOA injection. The complex envelope of the integrated gain modulation Δh is obtained in the form

$$\Delta h = \frac{L}{D(\Omega)} \Delta g, \quad (18)$$

where the expression of $D(\Omega)$ depends on which reduced model is considered. For the *DDE model* one obtains

$$\begin{aligned} D(\Omega) = {} & 1 - i\Omega\tau + \\ & + \frac{\tau P_{\rm in}}{E_{\rm sat}} \frac{h_0}{h_0 - \alpha_i L} \exp(h_0 - \alpha_i L)\left\{1 - R\exp(i\Omega t_g) + \right. \\ & + \left. R\exp(h_0 - \alpha_i L)\left[1 + \exp(i\Omega t_g)\right]\right\} + \\ & - \frac{\tau P_{\rm in}}{E_{\rm sat}} \frac{\alpha_i L}{(h_0 - \alpha_i L)^2}\left[\exp(h_0 - \alpha_i L) - 1\right] \\ & \left[1 + R\exp(h_0 - \alpha_i L)\right]. \end{aligned} \quad (19)$$

Note that the last term of $D(\Omega)$ in Eq. (19) is absent when the RSOA internal losses are negligible. The expression that is derived for the *ODE model* is

$$\begin{aligned} D(\Omega) = {} & 1 - i\Omega\tau + \frac{\tau P_{\rm in}}{E_{\rm sat}} \frac{h_0}{h_0 - \alpha_i L} \exp(h_0 - \alpha_i L) \\ & \left\{1 - R + 2R\exp(h_0 - \alpha_i L)\right\} + \\ & - \frac{\tau P_{\rm in}}{E_{\rm sat}} \frac{\alpha_i L}{(h_0 - \alpha_i L)^2}\left[\exp(h_0 - \alpha_i L) - 1\right] \\ & \left[1 + R\exp(h_0 - \alpha_i L)\right] \end{aligned} \quad (20)$$

and it can also be obtained from Eq. (19) by setting $t_g = 0$, i.e., by neglecting the signal propagation delay in the RSOA.

B. The Transparent Waveguide

The condition of transparency is characterized by the value of the integrated gain coefficient $h_0 = \alpha_i L$, which is a singular value of Eqs. (7) and (8). This case, yet of little practical relevance, is hence to be addressed separately. By defining the perturbation of $h(t)$ as $\delta h(t) = h(t) - h_0$, the analysis can be performed as illustrated for the case $h_0 \neq \alpha_i L$ provided that the following expansion is used in Eqs. (7) and (8):

$$\frac{\exp(h - \alpha_i L) - 1}{h - \alpha_i L} \simeq 1 + \frac{\delta h}{2}. \quad (21)$$

As a result, one obtains the following expression for the average value of the small signal gain coefficient:

$$\bar{g}_0 = \alpha_i \left[1 + \frac{\tau P_{\rm in}}{2E_{\rm sat}}(1 + R)\right], \quad (22)$$

which, when used along with Eq. (5), gives the value of the average injection current that is required in this case. The expression of $D(\Omega)$ for the *DDE model* reduces to

$$\begin{aligned} D(\Omega) = {} & 1 - i\Omega\tau + (1 + R)\frac{P_{\rm in}\tau}{E_{\rm sat}} \\ & \left\{1 + \frac{\alpha_i L}{2}\left[1 + \frac{2R}{1 + R}\exp(i\Omega t_g)\right]\right\}. \end{aligned} \quad (23)$$

The expression of $D(\Omega)$ for the *ODE model* is obtained by setting $t_g = 0$ in Eq. (23):

$$D(\Omega) = 1 - i\Omega\tau + (1 + R)\frac{P_{\rm in}\tau}{E_{\rm sat}}\left[1 + \alpha_i L\,\frac{1 + 3R}{2(1 + R)}\right]. \quad (24)$$

C. The Lossless Case

A case of particular interest is the lossless case, where the modulation coefficients can be conveniently expressed in an analytic, closed form. In fact, by setting $\alpha_i = 0$ and $R = 1$, Eq. (17) reduces to

$$\frac{h_0 - \overline{g}_0 L}{\tau} = -\frac{P_{\rm in}}{E_{\rm sat}}\left[\exp(2h_0) - 1\right], \quad (25)$$

which can be solved exactly in terms of the Lambert-W function W [18]. It is worth to remark that this function has come into view to provide analytic solutions in the study of the nonlinear regimes of other optical amplifiers, like Raman and Brillouin

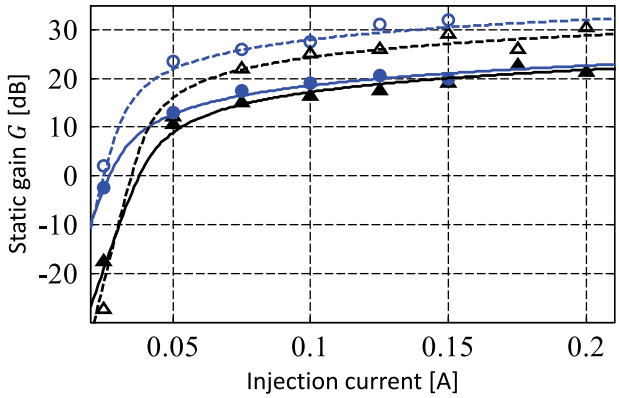

Fig. 1. The static gain $G = \exp(2h_0)$ as a function of the RSOA injection current. Markers show the experimental data from [6]: empty markers $\Gamma = 0.2$, filled markers $\Gamma = 0.8$, circles $L = 0.5$ mm, triangles $L = 0.7$ mm. The curves show the theoretical gain evaluated by using the expression for h_0 in Eq. (26): dashed curves for $\Gamma = 0.2$ (blue $L = 0.5$ mm; black $L = 0.7$ mm); solid curves for $\Gamma = 0.8$ (blue $L = 0.5$ mm; black $L = 0.7$ mm).

fiber amplifiers [19], [20], and might be applied also to the nonlinear regime of Erbium doped fiber amplifiers [21]. Eventually h_0 reads

$$h_0 = \overline{g}_0 L + \frac{\tau P_{\rm in}}{E_{\rm sat}} - \frac{1}{2} W\left[\frac{2\tau P_{\rm in}}{E_{\rm sat}} \exp\left(2\overline{g}_0 L + \frac{2\tau P_{\rm in}}{E_{\rm sat}}\right)\right]. \tag{26}$$

The expression of $D(\Omega)$ is then obtained by substituting Eq. (26) in Eqs. (19) and (20) for the DDE model and the ODE model, respectively, with $\alpha_i = 0$ and $R = 1$. For the ODE model, $D(\Omega)$ assumes a particularly simple form:

$$D(\Omega) = 1 - i\Omega\tau + W\left[\frac{2\tau P_{\rm in}}{E_{\rm sat}} \exp\left(2\overline{g}_0 L + \frac{2\tau P_{\rm in}}{E_{\rm sat}}\right)\right]. \tag{27}$$

Note that the RSOA static ($\Delta I = 0$) gain G is related to h_0 by $G = P_{\rm out}/P_{\rm in} = \exp(2h_0)$. In Fig. 1 we fit the functional dependence of the static gain on the injection current of the experimental data of Ref. [6] (markers) using Eq. (26) for h_0. The fitting has been realized by setting the parameters Γ and L to the values reported in [6], and by choosing the other parameters so as to fit the data. Herein after the decay rate is assumed to be given by the linear law $\mathcal{R}(N) = N/\tau$. Note that this choice, while simplifying the determination of analytic and numerical results, does not affect to any extent the validity of Eqs. (17), (19), and (20), which remain valid under different choices of $\mathcal{R}(N)$. In Fig. 1 the dashed curves are the theoretical results for the RSOA with $\Gamma = 0.2$, the blue curve for $L = 0.5$ mm, and the black curve for $L = 0.7$ mm. The other parameters are: $a = 8 \times 10^{-20}$ m^2, $N_0 \simeq 8 \times 10^{23}$ m^{-3}, $\tau = 300$ ps, $E_{\rm sat} \simeq 1$ pJ, $A = 1.17 \times 10^{-13}$ m^2 and input power $P_0 \simeq -11$ dBm (blue curve) and $P_0 \simeq -8$ dBm (black curve). The solid curves are the theoretical results for the RSOA with $\Gamma = 0.8$, the blue curve for $L = 0.5$ mm, and the red curve for $L = 0.7$ mm. The other parameters are: $a = 5 \times 10^{-20}$ m^2, $N_0 \simeq 2.5 \times 10^{23}$ m^{-3}, $\tau = 150$ ps, $E_{\rm sat} \simeq 0.64$ pJ, $A \simeq 2 \times 10^{-13}$ m^2 and input power $P_0 \simeq -1.5$ dBm (blue curve) and $P_0 \simeq -1$ dBm (red curve).

TABLE I
RSOA PARAMETERS

Description	Value
Active region cross-section area A	$350\ \mu$m$\times$ nm
Differential gain a	3×10^{-20} m^2
Group velocity v_g	8.33×10^7 m/s
Carrier lifetime τ	100 ps
Optical confinement factor Γ	0.3
Linewidth enhancement factor α	5

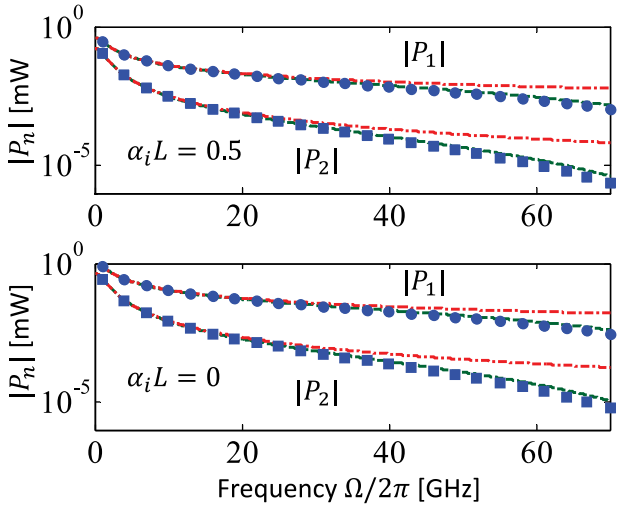

Fig. 2. Amplitudes of the first and second harmonics of the output field ($|P_1|$ and $|P_2|$, respectively) versus modulation frequency $\Omega/2\pi$ for a RSOA length of $L = 0.5$ mm. In the top panel the internal loss was set to $\alpha_i = 1$ mm^{-1}, in the bottom panel to $\alpha_i = 0$. The blue markers show the results obtained by solving the space-time equations (1)–(3); the dashed curves show the result of the DDE model; the dash-dotted curves show the result of the ODE model.

IV. Validation of the Analysis

In this section we first validate the analysis presented in Section III against numerical results obtained with the space-time model. To this aim Eqs. (1)–(3) were integrated with the method introduced in [22]. The RSOA parameter values used in the simulations are given in Table I (they are consistent with those used in [10]), whereas the optical carrier wavelength is set to 1550 nm.

In Figs. 2 and 3 we plot the amplitudes of the first and second harmonic of the output field intensity, $|P_1|$ and $|P_2|$, respectively, as a function of the modulation frequency $\Omega/2\pi$ for an input optical power of $P_{\rm in} = -10$ dBm. The blue markers show the results obtained by solving the space-time equations (1)–(3); the dashed curves show the result of the DDE model; the dash-dotted curves show the result of the ODE model. The RSOA length was set to $L = 0.5$ mm in Fig. 2 and to $L = 1$ mm in Fig. 3. In this example we assumed a perfectly reflective rear facet ($R = 1$), whereas the internal loss coefficient was set to $\alpha_i = 1$ mm^{-1} in the top panels of both figures, and to $\alpha_i = 0$ in the bottom panels. Finally, the average injection current was set to $\overline{I} = 1.2\, I_0$, and the modulation amplitude to $\Delta I = m_i I_0$, with a modulation depth $m_i = 0.1$. The agreement between both

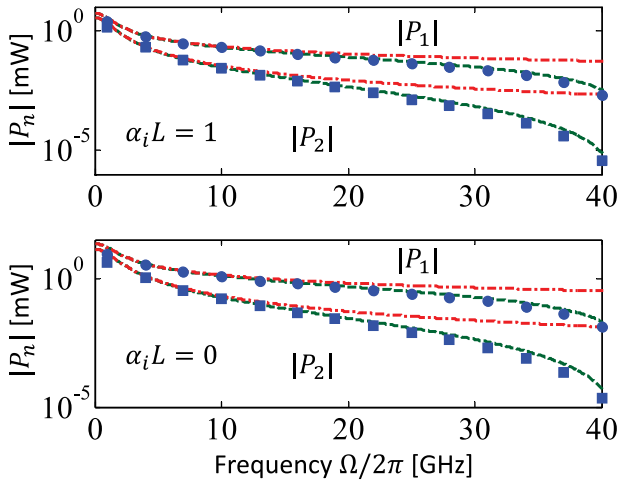

Fig. 3. Same as in Fig. 2 for a longer RSOA, $L = 1$ mm.

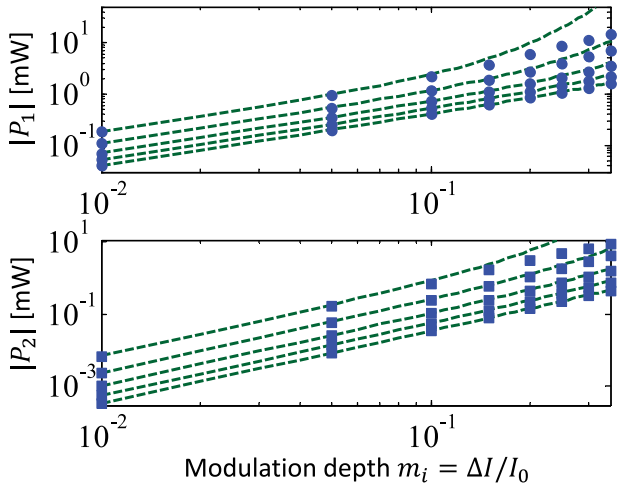

Fig. 4. Amplitudes of the first harmonic $|P_1|$ (top panel) and second harmonic $|P_2|$ (bottom panel) of the RSOA output optical power, versus modulation depth. The five curves, from top to bottom, were obtained using the DDE model for the frequency values $\Omega/2\pi = [1, 5, 10, 15, 20]$GHz. The markers refer to the space-time equations (1)–(3). The RSOA internal loss was set to $\alpha_i = 1$ mm^{-1}, whereas the other parameters were set to the same values as in Fig. 2.

reduced models and the space-time model in the low-frequency range is evident. At higher frequencies the DDE model is clearly more accurate.

In Fig. 4 we test the validity of the analysis with respect to the modulation depth. In the top and bottom panels we plot the values of $|P_1|$ and $|P_2|$, respectively, versus m_i. The five curves, from top to bottom, were obtained using the DDE model for the frequency values $\Omega/2\pi = [1, 5, 10, 15, 20]$ GHz (we omitted to plot the curves obtained for the ODE model, as they overlap with those obtained for the DDE model). The markers refer to the solutions of the space-time equations (1)–(3). The RSOA internal loss was set in this case to $\alpha_i = 1$ mm^{-1}, whereas the other parameters were set to the same values as in Fig. 2. The plot shows that the reduced model is always very accurate for

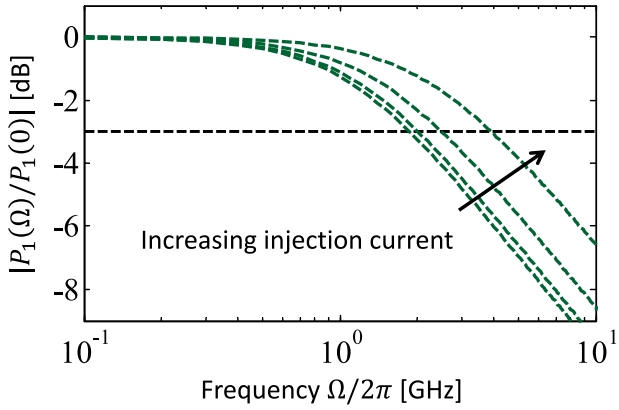

Fig. 5. Amplitude of the first harmonic $|P_1(\Omega)|$ normalized to $|P_1(0)|$ of the RSOA output optical power, versus the modulation frequency $\Omega/2\pi$. The four curves, from bottom to top, were obtained using the DDE model for the input current values $\overline{I} = [0.5, 1.5, 1.75, 2]\, I_0$. The RSOA internal loss was set to $\alpha_i = 1$ mm^{-1}, whereas the other parameters were set to the same values as in Fig. 2. The horizontal dashed curve shows the 3 dB reduction level.

values of m_i as large as about 0.1. For larger values it becomes less accurate at low frequencies.

Finally, we present in Fig. 5 the power of the first harmonic $|P_1(\Omega)|$ normalized to $|P_1(0)|$ as a function of the modulation frequency. The four curves were obtained using the DDE model and correspond to as many different values of the injection current, ranging from half to twice the transparency current value. The qualitative agreement of the modulation response with the experimental and numerical results observed for different devices [3], [4], [6], [7] is evident, and the 3 dB bandwidth increase with the injection current is captured.

V. Modulation Bandwidth

In this section we derive an expression for the RSOA modulation bandwidth, which we define as the frequency at which the amplitude of the first harmonic $|P_1|$ of the output optical power is reduced by 3 dB with respect to the value that it approaches in the limit of vanishingly small modulation frequencies. We denote the corresponding angular frequency by $\Omega_{3\mathrm{dB}}$. In the analysis we assume the ODE model. This choice is based on the remark that, as observable in Figs. 2 and 3, the ODE model matches very well both the DDE and space-time models for frequencies up to a few tens of GHz—values that certainly exceeds the sought bandwidth.

By observing Eq. (16) it can be noted that the only frequency dependent term in the formula for $|P_1|$ is K, the argument of the Bessel function. For the ODE model, i.e., Eq. (13) with $t_g = 0$, $K = 4|\Delta h(\Omega)|$. Hence, the condition fulfilled by the angular frequency $\Omega_{3\mathrm{dB}}$ is simply defined by the equation $I_1[4|\Delta h(\Omega_{3\mathrm{dB}})|] = I_1[4|\Delta h(0)|]/2$, where the term on the right hand side of the equality can be evaluated explicitly from the derived formulas. We verified that in a very broad range of RSOA parameters the Bessel function $I_1(x)$ ($x = 4|\Delta h(\Omega_{3\mathrm{dB}})|$) is very well approximated by its power expansion truncated at the third order. Using this expansion leaves

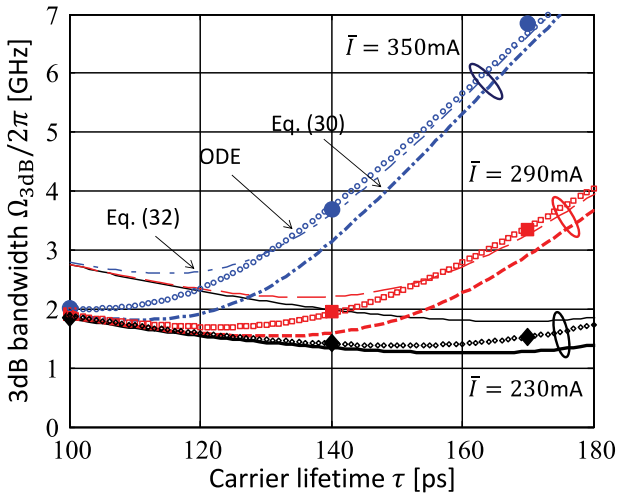

Fig. 6. Calculated 3 dB bandwidth versus carrier lifetime in a lossless RSOA ($\alpha_i = 0$, $R = 1$), for three values of the average injection current $\bar{I} = [230, 290, 350]$mA. Thick curves are the plot of Eq. (30), and thin curves show the corresponding limits for small current modulation given by Eq. (31), that in the lossless case coincides with (32). The small and the big markers show the numerical solutions of the ODE and space-time models, respectively.

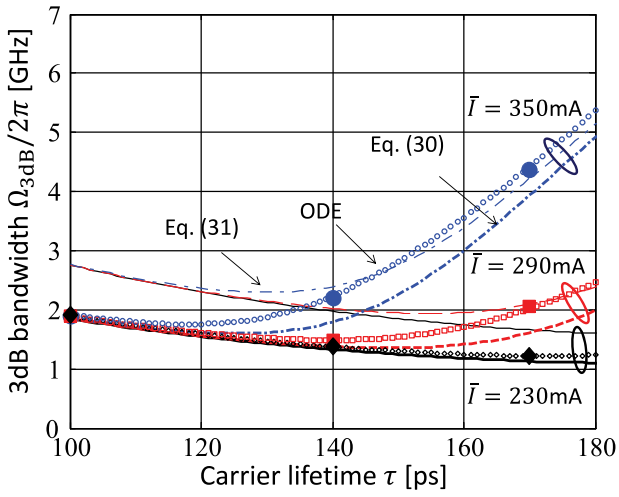

Fig. 7. Same as in Fig. 6, for a RSOA with an internal loss coefficient of $\alpha_i = 1$ mm^{-1} and a reflection coefficient at the rear facet of $R = 0.3$.

us with the resolution of the following polynomial equation

$$x^3 + px + q = 0, \tag{28}$$

where $p = 8$ and $q = -8I_1(4|\Delta h(0)|)/\Gamma(2)$ (where here Γ is the Gamma function), whose solution is given by Cardano's formula:

$$\begin{aligned} x = \; & (-q/2 + \sqrt{q^2/4 + p^3/27})^{(1/3)} \\ & + (-q/2 - \sqrt{q^2/4 + p^3/27})^{(1/3)}. \end{aligned} \tag{29}$$

The 3 dB angular frequency is finally obtained,

$$\Omega_{3\mathrm{dB}} = \frac{1}{\tau}\sqrt{\frac{16L^2}{x^2}|\Delta g|^2 - D_r^2}, \tag{30}$$

where D_r is the *frequency independent* real part of $D(\Omega)$ given by Eq. (20) for the general case and by Eq. (27) for the lossless case. Finally, by expanding all quantities to first order with respect to $|\Delta I|$, Eq. (30) reduces to the simpler expression

$$\Omega_{3\mathrm{dB}} = \sqrt{3}\frac{D_r}{\tau}, \tag{31}$$

which is independent from the modulation parameters.

In Figs. 6 and 7 the 3 dB bandwidth is presented as a function of the carrier lifetime τ, for three values of the average injection current $\bar{I} = [230, 290, 350]$ mA. Thick curves are the plot of Eq. (30), whereas thin curves show the corresponding limits for small current modulation given by Eq. (31). Fig. 6 refers to the lossless case ($\alpha_i = 0$ and $R = 1$), whereas in Fig. 7 the RSOA internal loss was set to $\alpha_i = 1$ mm^{-1} and the reflection coefficient to $R = 0.3$. In both figures the RSOA length was set to $L = 0.5$ mm, and the modulation depth to $m_i = \Delta I/I_0 = 0.1$, whereas the other parameters were: $P_{\mathrm{in}} = 1$ dBm; $E_{\mathrm{sat}} = 5$ pJ, $a = 3 \cdot 10^{-20}$ m^2, $\Gamma = 0.3$, $N_0 = 1.1 \cdot 10^{24}$ m^{-3}. The small and the big markers represent the numerical solutions of the ODE and of the space-time models, respectively. For the space-time model the 3 dB bandwidth was evaluated as the bandwidth at which the modulation amplitude $|P_1|$ drops to one half of the modulation amplitude evaluated at 100 MHz, a value below which the RSOA modulation response is practically flat, as shown in Fig. 5 (strictly speaking, this implies that the actual 3 dB bandwidth ranges between the analytic curves and the markers). The results obtained by numerically solving the ODE model and the space-time model are practically identical, which confirms the great accuracy of the reduced model. The agreement with the 3 dB bandwidth values given by Eq. (30)—considering the large modulation depth that was assumed—is also very good, with relative errors peaking at about 20%. The simpler formula of Eq. (31) is, as expected, less accurate, but preserves the correct dependence of the modulation bandwidth on the main RSOA parameters.

A. The Lossless Case

When setting $\alpha_i = 0$ and $R = 1$, Eq. (31) can be expressed as follows, in terms of the Lambert's W function

$$\Omega_{3\mathrm{dB}} = \frac{\sqrt{3}}{\tau}\left\{1 + W\left[\frac{2\tau P_{\mathrm{in}}}{E_{\mathrm{sat}}}\exp\left(2\bar{g}_0 L + \frac{2\tau P_{\mathrm{in}}}{E_{\mathrm{sat}}}\right)\right]\right\}. \tag{32}$$

The results obtained for the lossless case (that include those presented in [23]) are shown in Fig. 6. Equation (32) shows that when τ is sufficiently small the contribution of the W function is negligible (Lambert's $W(x)$ function is a monotonically increasing function of x, for $x > 0$, with $W(0) = 0$) and the bandwidth scales approximatively as $1/\tau$. However, when τ is large, the W function also increases and becomes dominant, due to the term $2\tau P_{\mathrm{in}}/E_{\mathrm{sat}}$ which represents the nonlinear RSOA saturation. From the physical viewpoint, this transition is a consequence of the fact that the carrier recombination induced by the nonlinear gain dynamics occurs at a faster rate when the RSOA is operated at relatively larger values of the bias current

as compared to the transparency current I_0 (which scales as $1/\tau$). The fact that a large τ would yield a large bandwidth is somehow counterintuitive, as typically it is assumed exactly the opposite, namely a large τ is considered to be a bandwidth limiting factor [2], [3]. As for the dependence of the simple 3 dB bandwidth formula on the increase of the operational parameters (i.e., the input optical power and bias current) we note that Eq. (32) yields the same qualitative growth found both in experimental [6] and numerical results [9] in the regime where the nonlinear gain saturation has not been reached.

B. The Transparent Waveguide

For the transparent waveguide Eq. (31) can be expressed as

$$\Omega_{3\mathrm{dB}} = \frac{\sqrt{3}}{\tau}\left\{1+(1+R)\frac{P_{\mathrm{in}}\tau}{E_{\mathrm{sat}}}\left[1+\alpha_i L\,\frac{1+3R}{2(1+R)}\right]\right\}, \tag{33}$$

as follows from using Eq. (24).

C. Comparison With the Modulation Response of a SOA in the Single-Pass Configuration

A natural question which arises when characterizing the modulation response of a RSOA is if there is any relation with the modulation response of single-pass devices. On this regard, we first note that the integrated gain of the reduced model of a SOA is the solution of Eq. (8) with $R = 0$. However, Eq. (8) for $R = 1$ can be recasted in the following form:

$$\frac{\mathrm{d}h'}{\mathrm{d}t} = -\frac{h'-g_0 2L}{\tau} - \frac{1}{E_{\mathrm{sat}}/2} \frac{h'}{h'-\alpha_i 2L}\left[\exp\left(h'-\alpha_i 2L\right)-1\right]|E_{\mathrm{in}}(t)|^2, \tag{34}$$

where $h' = 2h$ can be interpreted as the integrated gain of a single-pass SOA of length $2L$ and saturation energy $E_{\mathrm{sat}}/2$. This result suggests an interesting, non trivial property: the response of a perfectly reflective RSOA ($R = 1$) is identical (within the ODE model) to that of a single-pass SOA with double length, halved saturation energy and identical small-signal gain coefficient g_0. For instance in the case of bulk structures, this equivalence applies to a RSOA and a SOA of double length and halved cross section area (this leaves the transparency current, and hence the small-signal gain coefficient, unchanged).

We stress that the equivalence discussed above applies to SOAs with different geometrical characteristics. The comparison between the modulation bandwidths of a SOA operated in the single-pass and reflective configurations is addressed in Fig. 8. The thick and thin solid curves show the 3 dB bandwidth of a RSOA as given by Eq. (31) for decreasing values of the rear facet reflectivity R. The single-pass configuration, as pointed out in the beginning of this section, is described by the same equation in the limit $R = 0$, and is represented by the dashed curve. In the numerical example we set the average injection current to $\overline{I} = 290$ mA, and the internal loss coefficient to $\alpha_i = 1$ mm^{-1}. The figure shows that double-pass operation provides a larger modulation bandwidth than single-pass operation. We note that values of the 3 dB bandwidth corresponding to partial reflection at the RSOA rear facet ($0 < R < 1$) can also be achieved with a longer SOA, provided that the injection current is increased accordingly. As an example, the dotted curve in the figure shows the 3 dB-bandwidth of a SOA characterized by the same parameter values assumed for the RSOA, except for its length, which is set to twice the length of the RSOA and the bias current, which is doubled accordingly, so as to maintain the same injection current density or, equivalently, the same value of the ratio $\overline{I}/I_0$, which characterizes the SOA working point.

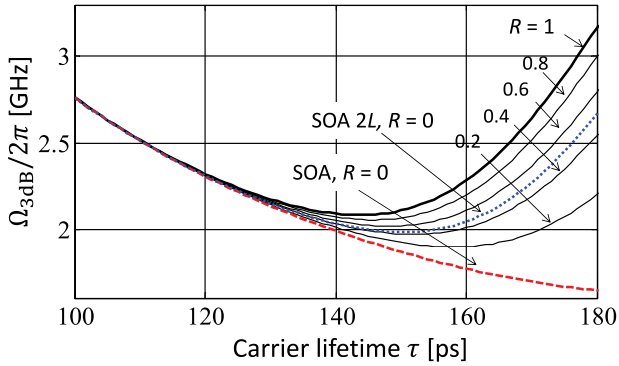

Fig. 8. The solid curves show the 3dB bandwidth given by Eq. (31) for a RSOA with internal loss coefficient $\alpha_i = 1\mathrm{mm}^{-1}$, average injection current $\overline{I} = 290$ mA, for several (displayed) values of the reflection coefficient R. The dashed curve shows the 3 dB bandwidth of a SOA with the same parameters operated in the single-pass configuration. The dotted curve is obtained by doubling the length of the single-pass SOA as well as the average injection current.

VI. Conclusion

The modulation response of a RSOA operated by modulating its injection current is studied by means of a previously published reduced model for the nonlinear response of RSOAs. In this paper we extended the reduced model so as to account for the RSOA internal loss and the partial mirror reflectivity and demonstrated the accuracy of the extended model over a very large frequency range. From the reduced model we derived an analytic expression of the corresponding 3 dB modulation bandwidth. The obtained expression greatly facilitates the study of the dependence of the modulation bandwidth on the RSOA parameters. One counter-intuitive dependence that we found is that an increase in bandwidth can be observed by increasing the carrier lifetime in the nonlinear saturation regime. Finally, we used the extended model to compare the modulation bandwidths of a SOA operated in the single-pass and reflective configurations.

Appendix
Introducing Loss in the Reduced Model

We define two delayed time reference frames, one moving at the group velocity of the forward propagating field $t_+ = t - z/v_g$, and another moving at the group velocity of the backward propagating field $t_- = t - (2L - z)/v_g$. In these

reference frames Eqs. (1) and (2) become:

$$\frac{\partial E_+}{\partial z} = -\frac{\alpha_i}{2}E_+ + \frac{1-i\alpha}{2}g_+E_+ \tag{35}$$

$$\frac{\partial E_-}{\partial z} = +\frac{\alpha_i}{2}E_- - \frac{1-i\alpha}{2}g_-E_-, \tag{36}$$

where E_+ and g_+ are explicit functions of z and t_+, whereas E_- and g_- are explicit functions of z and t_-, through the relations $E_+(z,t_+)=\tilde{E}_+(z,t_+ + z/v_g)$, $E_-(z,t_-)=\tilde{E}_-[z,t_- + (2L-z)/v_g]$, $g_+(z,t_+)=g(z,t_+ + z/v_g)$, and $g_-(z,t_-)=g[z,t_- + (2L-z)/v_g]$. Equations (35) and (36) have analytic solutions:

$$E_+(L,t_+) = \exp\left\{\frac{1-i\alpha}{2}h_+(t_+) - \frac{\alpha_i L}{2}\right\}E_+(0,t_+) \tag{37}$$

$$E_-(0,t_-) = \exp\left\{\frac{1-i\alpha}{2}h_-(t_-) - \frac{\alpha_i L}{2}\right\}E_-(L,t_-), \tag{38}$$

where we defined two auxiliary (real valued) functions

$$h_+(z,t_+) = \int_0^z g_+(z,t_+)\mathrm{d}z \tag{39}$$

$$h_-(z,t_-) = \int_z^L g_-(z,t_-)\mathrm{d}z, \tag{40}$$

and where, for the sake of brevity, we defined $h_+(t_+)\equiv h_+(L,t_+)$ and $h_-(t_+)\equiv h_-(0,t_-)$. At the RSOA rear facet $t_+=t_-$, and hence the boundary condition $\tilde{E}_-(L,t)=\sqrt{R}\tilde{E}_+(L,t)$ remains formally unchanged when expressed in the delayed time references, namely $E_-(L,t)=\sqrt{R}E_+(L,t)$. By making use of this condition, Eqs. (37)–(39) yield the following input-output relation for the electric field

$$E_-(0,t_-) = \sqrt{R}\exp\left\{\frac{1-i\alpha}{2}\left[h_+(t_-)+h_-(t_-)\right]-\alpha_i L\right\} E_+(0,t_-). \tag{41}$$

Following the procedure of [11], we proceed to derive an evolution equation for h_+. To this aim we first differentiate h_+,

$$\frac{\mathrm{d}h_+}{\mathrm{d}t_+} = \int_0^L \frac{\partial g_+(z,t_+)}{\partial t_+}\mathrm{d}z; \tag{42}$$

then, we substitute the right-hand side of Eq. (3) into the above integral, where all quantities are made explicit functions of z and t_+. This gives for h_+ the equation

$$\frac{\mathrm{d}h_+}{\mathrm{d}t_+} = -\frac{h_+ - g_0 L}{\tau} - \frac{1}{E_{\mathrm{sat}}}\int_0^L g_+(z,t_+)|E_+(z,t_+)|^2\mathrm{d}z - \frac{1}{E_{\mathrm{sat}}}\int_0^L g_-[z,t_+ - 2(L-z)/v_g] |E_-[z,t_+ - 2(L-z)/v_g]|^2\mathrm{d}z. \tag{43}$$

The evaluation of the second integral requires an approximation, as it cannot be reduced to any closed-form expression of h_+ and h_-. As already discussed in [11], for round-trip times smaller than the signal duration, a good approximation is obtained by replacing the z-dependent delay $2(L-z)/v_g$ with its average value $t_g = L/v_g$. Within this approximation the equation for h_+ simplifies to

$$\frac{\mathrm{d}h_+}{\mathrm{d}t_+} = -\frac{h_+ - g_0 L}{\tau} - \frac{1}{E_{\mathrm{sat}}}\int_0^L g_+(z,t_+)|E_+(z,t_+)|^2\mathrm{d}z - \frac{1}{E_{\mathrm{sat}}}\int_0^L g_-(z,t_+ - t_g)|E_-(z,t_+ - t_g)|^2\mathrm{d}z, \tag{44}$$

and, after replacing the two integrands with the expressions obtained from Eqs. (35) and (36), to

$$\begin{aligned}\frac{\mathrm{d}h_+}{\mathrm{d}t_+} = & -\frac{h_+ - g_0 L}{\tau} - \frac{1}{E_{\mathrm{sat}}}\left[|E_+(L,t_+)|^2 - |E_+(0,t_+)|^2\right] \\ & + \frac{1}{E_{\mathrm{sat}}}\left[|E_-(L,t_+ - t_g)|^2 - |E_-(0,t_+ - t_g)|^2\right] \\ & - \frac{\alpha_i}{E_{\mathrm{sat}}}\int_0^L |E_+(z,t_+)|^2\mathrm{d}z \\ & - \frac{\alpha_i}{E_{\mathrm{sat}}}\int_0^L |E_-(z,t_+ - t_g)|^2\mathrm{d}z.\end{aligned} \tag{45}$$

We then use Eqs. (37) and (38), as well as the boundary condition $E_+(L,t)=E_-(L,t)$, to obtain

$$\begin{aligned}\frac{\mathrm{d}h_+}{\mathrm{d}t_+} = & -\frac{h_+ - g_0 L}{\tau} - \frac{1}{E_{\mathrm{sat}}}\left[\exp(h_+ - \alpha_i L) - 1\right]|E_+(0,t_+)|^2 \\ & - \frac{R}{E_{\mathrm{sat}}}\left\{\exp[h_-(t-t_g) - \alpha_i L] - 1\right\}\exp[h_+(t-t_g) \\ & - \alpha_i L]|E_+(0,t_+ - t_g)|^2 - \frac{\alpha_i}{E_{\mathrm{sat}}}\int_0^L |E_+(z,t_+)|^2\mathrm{d}z \\ & - \frac{\alpha_i}{E_{\mathrm{sat}}}\int_0^L |E_-(z,t_+ - t_g)|^2\mathrm{d}z.\end{aligned} \tag{46}$$

We now derive a relation between h_- and h_+ by noting that $g_-(z,t)=g_+[z,t+2(L-z)/v_g)$ and hence

$$h_-(t_-) = \int_0^L g_+[z,t_- + 2(L-z)/v_g]\mathrm{d}z. \tag{47}$$

Like in the derivation of Eq. (44), we approximate $2(L-z)/v_g$, i.e., the second term in the argument of g_+, by its average value t_g, to obtain

$$h_-(t_-) \simeq h_+(t_- + t_g). \tag{48}$$

We note that using this relation in Eq. (41), and returning to the absolute time reference at $z=0$, gives the input-output relation in the form

$$\tilde{E}_-(0,t_- + 2t_g) = \sqrt{R}\exp\left\{\frac{1-i\alpha}{2}\left[h_+(t_- + 2t_g) + h_+(t_- + t_g)\right] - \alpha_i L\right\}\tilde{E}_+(0,t_-), \tag{49}$$

which can be seen to be equivalent to Eq. (6) after defining $t = t_- + 2t_g$, $E_{\mathrm{in}}(t)=\tilde{E}_+(0,t)$, and $E_{\mathrm{out}}(t)=\tilde{E}_-(0,t)$, and by replacing h_+ with h for simplifying the notation.

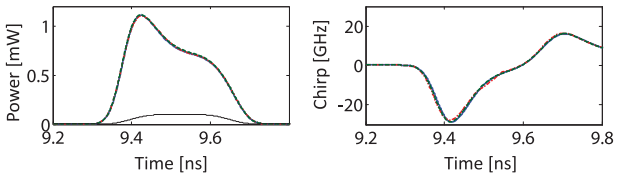

Fig. 9. Output power (left) and chirp (right) for the tenth pulse of an input pulse train with 1 GHz repetition rate. Solid curves show the numerical solution of the space-time model, Eqs. (1)–(3); dashed curves show the solution of the DDE reduced model; dash-dotted curves show the solution of the ODE reduced model. The thin dotted curve in the left panel shows the input pulse power. The RSOA internal loss coefficient was set to $\alpha_i = 1$ mm^{-1} and the power reflection coefficient at the rear facet to $R = 0.5$. The other parameters used in this example are given in the main text.

Substituting this relation in Eq. (46) yields

$$\frac{\mathrm{d}h_+}{\mathrm{d}t_+} = -\frac{h_+ - g_0 L}{\tau} - \frac{1}{E_{\mathrm{sat}}}\left[\exp(h_+ - \alpha_i L) - 1\right]\left\{|E_+(0,t_+)|^2 + R\exp[h_+(t-t_g) - \alpha_i L]|E_+(0,t_+ - t_g)|^2\right\} - \frac{\alpha_i}{E_{\mathrm{sat}}}\int_0^L |E_+(z,t_+)|^2 \mathrm{d}z - \frac{\alpha_i}{E_{\mathrm{sat}}}\int_0^L |E_-(z,t_+ - t_g)|^2 \mathrm{d}z. \quad (50)$$

We are left with the evaluation of the two integrals in Eq. (50). To this aim we approximate the integrated gain functions $h_+(z,t_+)$ and $h_-(z,t_-)$ to first order in z around $z = 0$ and $z = L$, respectively,

$$h_+(z,t_+) = \int_0^z g_+(z',t_+)\mathrm{d}z' \simeq z\, g_+(0,t_+), \quad (51)$$

$$h_-(z,t_-) = \int_z^L g_-(z',t_-)\mathrm{d}z' \simeq (L-z)\, g_-(L,t_-). \quad (52)$$

With this approximation, the first integrand can be expressed as

$$|E_+(z,t)|^2 = \exp\left\{[g_+(0,t) - \alpha_i]z\right\}|E_+(0,t)|^2 \quad (53)$$

and so

$$\int_0^L |E_+(z,t)|^2 \mathrm{d}z = L\frac{\exp\{h_+ - \alpha_i L\} - 1}{h_+ - \alpha_i L}|E_+(0,t)|^2. \quad (54)$$

Similarly, the second integrand can be expressed as

$$|E_-(z,t)|^2 = \exp\left\{[g_-(L,t) - \alpha_i](L-z)\right\}|E_-(L,t)|^2 \quad (55)$$

and so

$$\int_0^L |E_-(z,t)|^2 \mathrm{d}z = L\frac{\exp\{h_- - \alpha_i L\} - 1}{h_- - \alpha_i L}|E_-(L,t)|^2. \quad (56)$$

Eventually Eq. (7) is obtained by using Eqs. (54) and (56) in Eq. (50), as well as Eq. (48) and the relation $|E_-(L,t_+ - t_g)|^2 = R|E_+(0,t_+ - t_g)|^2 \exp\left[h_+(t_+ - t_g) - \alpha_i L\right]$ which follows from the boundary conditions and from Eq. (37).

To demonstrate the accuracy of the model which includes losses, we simulated the amplification of a 1 GHz-periodic pulse train consisting of unchirped input pulses with a second order super-Gaussian intensity profile. In Fig. 9 we plot by solid curves the output power (left panel) and chirp (right panel) obtained by numerically integrating Eqs. (1)–(3) with the method introduced in [22]. The RSOA parameters were set as follows: $L = 1$ mm, $g_0 = 3000\,\mathrm{m}^{-1}$, $E_{\mathrm{sat}} = 5$ pJ, $\alpha_i = 1\,\mathrm{mm}^{-1}$, $R = 0.5$. The input pulse energy was set to $E_{\mathrm{sat}}/10$. Dashed curves show the solutions of the DDE reduced model; dash-dotted curves are the solutions of the ODE reduced model. The thin dotted curves show the input pulse intensity. The excellent agreement between the results obtained using the space-time model and those obtained by using the reduced models is evident.

ACKNOWLEDGMENT

The authors would like to thank an anonymous reviewer for the insightful comments.

REFERENCES

[1] P. P. Iannone and K. C. Reichmann, "Optical access beyond 10 Gb/s PON," presented at the Eur. Conf. Exhib. Optical Communications, Turin, Italy, 2010, Paper Tu.3.B.1.

[2] H.-S. Kim, B.-S. Choi, K.-S. Kim, D. C. Kim, O.-K. Kwon, and D.-K. Oh, "Improvement of modulation bandwidth in multisection RSOA for colorless WDM-PON," *Opt. Exp.*, vol. 17, pp. 16372–16378, 2009.

[3] G. de Valicourt, "Next Generation of Optical Access Network Based on Reflective-SOA," *Selected Topics Optical Amplifiers Present Scenario*, Sisir Garai Ed. Rijeka, Croatia: InTech, 2012.

[4] K. Y. Cho, Y. Takushima, and Y. C. Chung, "10-Gb/s Operation of RSOA for WDM PON," *IEEE Photon. Technol. Lett.*, vol. 20, no. 18, pp. 1533–1535, Sep. 2008.

[5] B. Schrenk, G. de Valicourt, M. Omella, J. A. Lazaro, R. Brenot, and J. Prat, "Direct 10-Gb/s modulation of a single-section RSOA in PONs with high optical budget," *IEEE Photon. Technol. Lett.*, vol. 22, no. 6, pp. 392–394, Mar. 2010.

[6] G. de Valicourt *et al.*, "Radio-over-fiber access network architecture based on new optimized RSOA devices with large modulation bandwidth and high linearity," *IEEE Trans. Microw. Theory Technol.*, vol. 58, no. 11, pp. 3248–3258, Nov. 2010.

[7] Y. Zhan, M. Zhang, J. Zhan, L. Liu, M. Liu, and X. Chen, "Analysis and experimented on frequency response characteristics of RSOA based on small signal analysis method," presented at the Communication Photon. Conf., Guangzhou, China, Paper AF 4A.24.

[8] M. J. Connelly, "Wide-band steady-state numerical model and parameter extraction of a tensile-strained bulk semiconductor optical amplifier," *IEEE J. Quantum Electron.*, vol. 43, no. 1, pp. 47–56, Jan. 2007.

[9] A. R. Totović, J. V. Crnjanski, M. M. Krstić, and D. M. Gvozdić, "Numerical study of the small-signal modulation bandwidth of reflective and traveling-wave SOAs," vol. 33, no. 13, pp. 2758–2764, Jul. 2015.

[10] J. Mork, A. Mecozzi, and G. Eisenstein, "The Modulation response of a semiconductor laser amplifier," *IEEE J. Sel. Topics Quantum Electron.*, vol. 5, no. 3, pp. 851–860, May/Jun. 1999.

[11] C. Antonelli and A. Mecozzi, "Reduced model for the nonlinear response of reflective semiconductor optical amplifiers," *IEEE Photon. Technol. Lett.*, vol. 25, no. 23, pp. 2243–2246, Dec. 2013.

[12] L. A. Coldren, S. W. Corzine, and M. L. Mašanović, *Diode Lasers and Photonic Integrated Circuits*, New York, NY, USA: Wiley, 2012, Ch. 4, p. 223.

[13] G. P. Agrawal and N. A. Olsson, "Self-phase modulation and spectral broadening of optical pulses in semiconductor laser amplifiers," *IEEE J. Quantum Electron.*, vol. 25, no. 11, pp. 2297–2306, Nov. 1989.

[14] C. B. Su, "Nonlinear gain caused by cavity standing wave dielectric grating as an explanation of the relationship between resonance frequency and damping rate of semiconductor diode lasers," *Appl. Phys. Lett.*, vol. 53, pp. 950–952, 1988.

[15] S. P. O Duill and L. P. Barry, "Improved reduced models for single-pass and reflective semiconductor optical amplifiers," *Opt. Commun.*, vol. 334, pp. 170–173, 2015.

[16] A. Mecozzi and J. Mørk, "Saturation induced by picosecond pulses in semiconductor optical amplifiers," *J. Opt. Soc. Amer. B*, vol. 14, pp 761–770, 1997.

[17] M. Abramowitz and I. A. Stegun, *Handbook of Mathematical Functions with Formulas, Graphs, and Mathematical Tables*, New York, NY, USA: Dover, 1965, Ch. 9.

[18] R. M. Corless *et al.*"On the Lambert W function," *Adv. Comput. Math.*, vol. 5, pp. 329–359, 1996.
[19] M. Santagiustina, "Exact integral solution of saturation and depletion in forward and backward optical fiber Raman amplifiers," *Opt. Lett.*, vol. 32, pp. 3023–3025, 2007.
[20] M. Santagiustina, "Exact, implicit, integral solution of depletion and saturation in Raman and Brillouin fiber amplifiers," presented at the European Conf. Lasers Electro-Optics, Int. Quantum Electronics Conf., Munich, Germany, 2007, Paper CJ-20-Tue.
[21] M. Peroni and M. Tamburrini, "Gain in Erbium-doped fiber amplifiers: A simple analytical solution for the rate equations," *Opt. Lett.*, vol. 15, pp. 842–844, 1990.
[22] J. W. D. Chi, L. Chao, and M. K. Rao, "Time-domain large-signal investigation on nonlinear interactions between an optical pulse and semiconductor waveguides," *IEEE J. Quantum Electron.*, vol. 37, no. 10, pp. 1329–1336, Oct. 2001.
[23] C. Antonelli, A. Mecozzi, Z. Hu, and M. Santagiustina, "Analytical expression for the modulation bandwidth of a reflective semiconductor optical amplifier," presented at the 12th Int. Conf. Fiber Optics Photon., Kharagpur, India, 2014, Paper T2B.5.

Cristian Antonelli received the M.Sc. and Ph.D. degrees in electrical engineering from the University of L'Aquila, L'Aquila, Italy, in 2002 and 2006, respectively. During the Graduate degree, he worked on the "Hinge Model" for the time dynamics of PMD in lightwave systems with a collaboration with AT&T Labs, NJ, USA, where he was a Visiting Scientist in the summers of 2004 and 2005. In 2006, he spent six months with the Research Laboratory of Electronics Massachusetts Institute of Technology, performing research on the theory of mode-locked fiber lasers. Since 2007, he has been a Senior Research Scientist, first with Consorzio Nazionale Interuniversitario per le Scienze Fisiche della Materia, the Italian Interuniversity Consortium for the Physics of Matter, Catania, Italy, and then with the University of L'Aquila, where he joined the Department of Physical and Chemical Sciences as an Assistant Professor, in April 2014. His research interests include the modeling and characterization of fiber-optic communication systems, including PMD and PDL, fundamental energy consumption limits, semiconductor optical amplifier-based devices, and linear and nonlinear propagation effects in space-division multiplexed transmission. He is currently a TCP Member for OFC 2016, as well as an Associate Editor for *Journal of Lightwave Technology*.

Antonio Mecozzi (F'03) is currently a Professor and the Director of the Department of Physical and Chemical Sciences of the University of L'Aquila, L'Aquila, Italy. Previously, he was with the Optical Communication Division of Fondazione Ugo Bordoni Rome, Italy. From 1991 to 1992, he was a Visiting Scientist with the Department of Electrical Engineering and Computer Science and the Research Laboratory of Electronics of Massachusetts Institute of Technology. His research interests include studies on soliton transmission, laser mode-locking, nonlinear propagation in single and multimode fibers, modal dispersion in multimode fibers, physics and applications of semiconductor optical amplifiers, and optical amplification and noise. He holds numerous patents and more than 160 publications in refereed scientific journals. He is currently an Associate Editor for the *Optics Express*. He is a Fellow of the Optical Society of America.

Zhefeng Hu received the B.S. degree in mechanics engineering and the Ph.D. degree in electronic science and technology from the Huazhong University of Science and Technology, Wuhan, Hubei, China, in 2002 and 2010, respectively. In 2010, he was a Lecturer (Assistant Professor) with the University of Electronic Science and Technology of China (UESTC), Sichuan, China. From 2013 to 2014, he was a Postdoctoral Research Fellow with the University of Padova. After that he returned to China and continued his work at UESTC. His research interests include all-optical signal processing, passive optical networks, optical waveguides, and microwave photonics.

Marco Santagiustina was born in Venice, Italy, in 1966. He received the Laurea (Hons.) degree in electronic engineering, and the Ph.D. degree in telecommunication engineering from the University of Padova, Padova, Italy, in 1992 and 1996, respectively. He was a Visiting Scholar with the Optical Sciences Center, University of Arizona, Tucson, USA, as a Fulbright Grant holder in 1995. In 1996, he was Visiting Research Lecturer with the University of New Mexico, Albuquerque, USA, and a Visiting Scholar at Brown University, Providence, RI, USA, under an US Air Force grant. From 1997 to 1999, he was Postdoctoral Researcher with the University of the Balearic Islands, Spain, under a European Training and Mobility of Researcher Program. Since 1999, he has been with the Department of Information Engineering, University of Padua, Padua, Italy, first as a permanent Research Fellow, and from 2011, as an Associate Professor. His main research interests include nonlinear optics and optical communications. He is the author or coauthor of more than 110 articles and memories published in international scientific reviews, books, and proceedings of international conferences, and holds one International patent. He was the Coordinator of the FP7, FET-Open Project GOSPEL, of one international bilateral project, of two national research projects and three projects financed by the University of Padova. He has been collaborating in several national (PFT) and international research projects. He is a Reviewer for the IEEE PHOTONICS TECHNOLOGY LETTERS, *Journal of Lightwave Technology*, *Optics Letters*, *JOSA B*, *Optics Express*, *Optics Communications, Physical Review Letters, Physical Review E,* and *the European Journal of Optics*. He is a TPC Member at ECOC 2015.